

A numerical investigation of a combined solar chimney and water wall for building ventilation

H. Wang and C. Lei

Centre for Wind, Waves and Water, School of Civil Engineering
 The University of Sydney, New South Wales 2006, Australia

Abstract

In this paper, a combined solar chimney and water wall is numerically investigated for mild winter weather conditions in Sydney, Australia. It is found that, compared with a conventional solar chimney, a window-sized unit of the proposed system extends the ventilation effects by more than 3 hours and helps to maintain the warmth of the room during the night. The effects of the air gap width on the thermal performance of the combined system are examined. The results suggest that, as the air gap width decreases, the room temperature increases at the cost of reduced ventilation rate. Considering that the reduced ventilation rate resulting from the reduction of the air gap width is still sufficient for ventilating the indoor space, it is advisable to use relatively small air gap widths for the considered climate conditions.

Introduction

Solar chimney is a natural ventilation strategy that takes advantage of solar heat to induce ventilation for the indoor space to which it is attached. Solar chimney has gained global recognition during the last few decades as an effective natural ventilation strategy. However, some issues related to solar chimney have not been fully addressed. Firstly, with solar heat as the only energy source, solar chimney stops working immediately after sunset. In addition, in order to maximize the capture of solar heat, solar chimney usually stands on the sun-facing side of the building and deprives the building of natural lighting. In order to reduce the negative impacts of these two drawbacks, the present authors introduced a modified solar chimney with a water wall taking the place of its absorber wall [1]. During the day, part of the solar radiation reaching the solar chimney is absorbed and stored by the water wall while the rest of the sunlight is allowed into the room to satisfy the need for daylighting. After the sunset, the heat stored in the water wall is released to both the solar chimney and the room. As a result, the ventilation effect of the solar chimney and the warmth level of the indoor environment are both sustained. In this paper, the thermal performance of the combined system is numerically studied under mild winter weather conditions in Sydney, Australia. The impacts of the air gap width on the performance of the proposed system are also considered.

Problem Formulation

Due to the constraints of available computational resources, the present study only considers a two-dimensional (2D) combined solar chimney and water wall system, which may represent a cross-section of a real-life prototype. It is assumed that the boundary effects can be neglected, and thus the 2D model is expected to indicate the typical performance of the real-life prototype. The schematic of the 2D model under consideration is shown in Figure 1. As illustrated in the figure, a 2D combined solar chimney and water wall system is installed at the centre of the sun-facing wall of a 3m×3m room while the room inlet vent is installed at the bottom of the opposite wall. In order to prevent rain or snow from coming into the indoor space through the openings, caps are installed on the top of the chimney outlet and

at the room inlet. It is assumed that the length of the caps sticking out of the envelop of the combined system is 0.2m.

In order to simplify the problem, it is assumed that reflection of solar radiation and long-wave radiation between the two opposing solid surfaces can be neglected. As such, the attenuation of solar radiation across the system is assumed to be along the horizontal direction and follow Beer's Law. Hence, if the amount of solar radiation reaching the external surface of a participating medium, such as the glass panel or the water column, is I , after traveling in the media for a distance of L , the residual radiation becomes $Ie^{-\eta L}$, where η represents the attenuation coefficient. According to Lei et al. [2], the attenuation coefficient of water is set to 6.16m^{-1} . Conventional engineering calculations are performed to ensure the glass panel thickness provides sufficient strength against water pressure and the results suggest that glass thickness greater than 18mm is appropriate. In this study, 25mm (1 in) is adopted and the corresponding solar transmission rate is 0.516 (refer to Rubin [3]). The reference case is defined such that both the air gap width (d_c) and the water column thickness (d_w) are 0.2m. Considering that solar radiation reaching the room is first absorbed by the walls and is consequently transferred to the room air, it is assumed that any residual solar radiation is absorbed by the room air.

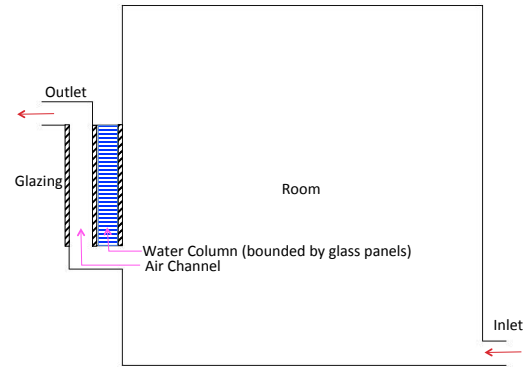


Figure 1. Schematic of the combined solar chimney and water wall system

According to Wu and Lei [4], typical mild winter weather conditions in Sydney, Australia can be approximated by the following equations:

Ambient temperature:

$$T_a(t) = T_0 + 0.5\Delta T \sin\left[\frac{2\pi(t-t_{lag})}{P}\right] \quad (1)$$

Solar radiation:

$$I(t) = \begin{cases} I_{max} \sin\left(\frac{2\pi t}{P}\right) & \text{for } (m-1)P < t < (m-\frac{1}{2})P \\ 0 & \text{for } (m-\frac{1}{2})P < t < mP \end{cases} \quad (2)$$

where $T_0 = 12.5^\circ\text{C}$ is the daily average temperature, $\Delta T = 15^\circ\text{C}$ the daily temperature fluctuation, $t_{lag} = 2\text{h}$ the time lag between the peak of ambient temperature and that of solar radiation, $I_{max} = 800\text{W}/\text{m}^2$ the daily maximum solar radiation intensity and $P = 24\text{h}$ the duration of a thermal cycle. A

thermal cycle is equivalent to a day except for the fact that a thermal cycle starts at 6am ($t=0h$) and ends at 6am the next day ($t=24h$). It is clear that each day solar radiation lasts for 12 hours ($t=0$ to 12h) and for the rest of the day solar radiation intensity is kept at zero. Daily peak of solar radiation can be observed at $t=6h$, which corresponds to the midday. On the other hand, the ambient temperature varies between 5°C and 20°C and reaches its maximum and minimum at $t=8h$ (2pm) and 20h (2am) respectively. It is worth noting that the above climate condition is highly simplified. This is justified since the present investigation focuses on fundamental understanding of the response of the combined water wall and solar chimney system to diurnal forcing rather than its design and optimization for specific climate conditions.

These weather conditions are adapted into boundary conditions with a commercial computational fluid dynamics (CFD) solver ANSYS Fluent. Solar radiation absorbed by each component is converted into source terms and are thus accounted for through the energy equations. The boundary conditions for the inlet and outlet are pressure inlet and pressure outlet respectively. In order to simplify the problem, it is assumed that the combined system is an isolated structure and therefore the effect of surrounding environment is not considered. On the other hand, it is assumed that wind has negligible impact on the system. Accordingly, the gauge pressures at the inlet and outlet are set to 0 while the temperature is set to the ambient temperature.

In the present study, heat transfer between the glazing and the ambient environment is via convection and radiation. According to McAdams [5], the convective heat transfer coefficient at the external surface of a building envelope can be estimated by the following equation:

$$h_a^{conv} = 5.7 + 3.8V_{wind} \quad (3)$$

where V_{wind} is the wind speed. In this study, $V_{wind} = 0$, and thus h_a^{conv} is constant. On the other hand, the radiative heat transfer at the glazing-ambient interface is idealized to occur between the surface temperature of the glazing and an effective external radiation temperature, which, following the procedures reported by Goia et al. [6], can be calculated by:

$$T_{ext,rad} = \left(\frac{\sqrt{2}}{4} T_{sky}^4 + \frac{2-\sqrt{2}}{4} T_{air}^4 + \frac{1}{2} T_{ground}^4 \right)^{\frac{1}{4}} \quad (4)$$

where T_{sky} , T_{air} and T_{ground} are sky temperature, air temperature and ground temperature respectively. The air temperature and ground temperature are assumed to be equal and can both be computed from equation (1) while T_{sky} can be approximated by $T_{sky} = 0.0522T_{air}^{1.5}$.

Given the complexity of the geometry of the air domain and the time-varying behavior of the heating conditions, it can be anticipated that turbulent flow structure would be remarkable during some specific time period, if not all the time. Therefore, a turbulence model is adopted. In this study, the one-equation Spalart-Allmaras (S-A) model is adopted because of its good performance in predicting natural convections and the savings in computational resources (refer to Abraham and Sparrow [7], Paitoonsurikarn and Lovegrove [8], Yuan et al. [9], Ohk and Chung [10]). The detailed formulation of this model can be found in Spalart and Allmaras [11]. The first-order implicit scheme is adopted for transient formulation, while SIMPLEC (semi-implicit method for the pressure linked equations-consistent) scheme (refer to Van Doormaal and Raithby [12]) with skewness correction is selected as the pressure-velocity coupling method. Spatial discretization scheme for pressure is PRESTO! (pressure staggering option) (refer to Fluent [13]) while the spatial

discretization scheme for both momentum and energy equations is by the second-order upwind scheme.

In order to work out the adequate spatial and temporal resolutions to solve the problem, mesh and time-step tests are performed to find the optimum combination. Considering that solar chimney channel is where significant heat transfer takes place and where buoyancy-driven flow originates, in order to reduce the need for computational resources, mesh and time-step dependence tests are performed only for the solar chimney channel with one wall heated with a heat flux of I_{max} and the other thermally insulated. The results show that a time-step of 1s and a 90×100 mesh with wall cell thickness of 0.15mm is adequate to fully resolve the problem. The wall cell thickness also satisfies the y^+ requirement of the S-A model ($y^+ \sim 1$) (refer to Fluent [13]). Hence, in the following chapters, a time-step of 1s and a mesh grid with comparable spatial resolution for the whole system are adopted, excluding the room domain where reasonably coarser mesh is used to save computational time.

In order to eliminate start-up effects and understand the typical performance of the combined system under the weather conditions defined by equations (1) and (2), CFD calculations on the proposed model are performed until quasi-equilibrium is achieved. In this study, it is assumed that quasi-equilibrium is reached as soon as the root mean square errors (RMSE) between two consecutive thermal cycles drops to below 1% of the daily fluctuation of the corresponding quantities.

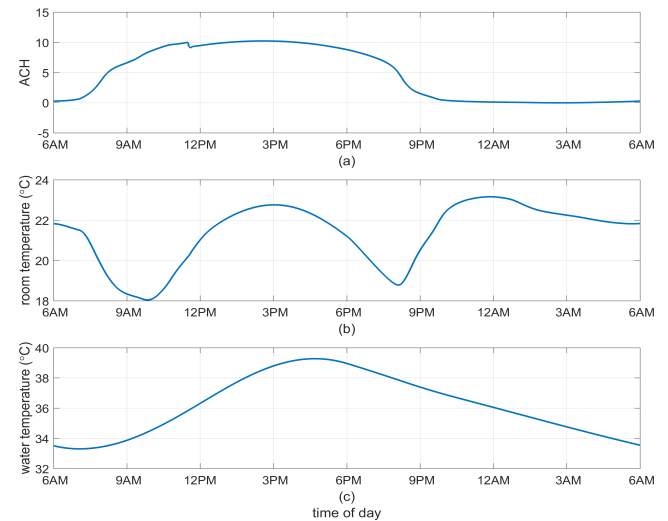


Figure 2. CFD results for predicted (a) ventilation rate, (b) room temperature and (c) water temperature.

Results and Discussions

Reference case

Quasi-equilibrium performance of the reference case is plotted in Figure 2. The corresponding temperature distribution and streamlines across the system at sunrise, noon, sunset and midnight are displayed in Figure 3 and Figure 4 respectively. The ventilation flow rate is calculated at the chimney outlet and is converted to air change per hour (ACH) through $ACH = \frac{\dot{m} \times 3600}{\rho V}$ where \dot{m} is the mass flow rate in kg/s, ρ the average density at chimney outlet in kg/m^3 and V the room volume in m^3 . Although the combined system under investigation is 2D, when calculating the ACH of the system the depth of the solar chimney and water wall is assumed to be 1m while that of the room is 3m. In this way, the thermal performance of a window-sized combined system attached to a room of typical size (*i.e.* $V=27m^3$) can be obtained.

It can be seen from Figure 2(a) that, as solar radiation increases, the ventilation rate also increases except for a short period of time between 11:30am and 12:00pm. However, even if solar radiation starts to decline after its peak at noon, the ventilation rate still increases for another 2.25 hours before it reaches the daily maximum. According to CIBSE [14], in order to provide sufficient ventilation for a residential indoor space, a ventilation rate of 1ACH is required. It is clear that, with daily average ventilation rate calculated to be 4.72ACH, the combined system is more than capable of providing ventilation for the indoor space. The present calculation results indicate that for over 14 hours a day the ventilation rate is greater than 1ACH, out of which almost 3.4 hours are during the night. This result serves as a proof that the proposed system is capable of extending the ventilation effects into the night. On the other hand, it can be seen from Figure 2(b) that, the combined system plays a significant role in maintaining the warmth of the room as well as in reducing the daily room temperature fluctuations. Compared with the ambient temperature that ranges between 5°C and 20°C throughout the day, the room temperature is maintained at a daily average of 21.35°C with a daily fluctuation of only 5.12°C.

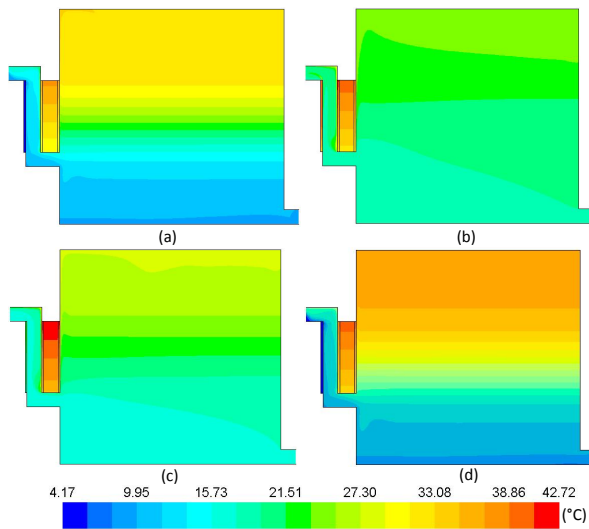


Figure 3. Temperature contours at (a) sunrise, (b) midday, (c) sunset and (d) midnight

It can be seen from Figure 3 (a) and Figure 4 (a) that, at sunrise, due to heat loss at the glazing, reverse flow offsets the buoyancy-driven flow near the water wall and penetrates into the room. At this stage, with little ventilation effect generated in the solar chimney, the circulation of room air is rather weak, and as a result, heat transferred from the water wall accrues in the top part of the room, leading to a significant thermal stratification. As solar radiation increases, temperature of the glazing and subsequently the ventilation rate rapidly grows because of the absorption of solar radiation. With cooler ambient air constantly being drawn into the room, the room temperature decreases in the first place but finally increases. This phenomenon is caused by the improved mixing of the room air and the absorption of residual solar heat, as can be observed at midday in Figure 3 (b) and Figure 4 (b). In the meantime, the vortex near the inlet that is clearly seen in Figure 4(a) is gradually entrained to the left by the ventilating flow and is eventually suppressed after it reaches the lower left corner of the room. In order to bypass the vortex, the ventilating flow takes a detour before it enters the chimney channel, which causes a slight reduction of the ventilation rate around 11:30am in Figure 2(a). After the midday, due to the decline of solar radiation, heating of the room air has a stronger dependence on the water wall. With the heating from the water wall, the room temperature continues to increase until around

3pm when the cooling effects of the incoming ambient air starts to prevail. It can be seen from Figure 3 (c) and Figure 4 (c) that at sunset room air circulation is weakened and as a result thermal stratification builds up in the room. This observation can be explained by the decline of the ventilation effects due to the continuous heat loss through the glazing. In the meantime, compared with the situation at noon, incoming air flows across a larger part of the room, spreading out its cooling effects, which partly explains the temperature decrease during this period. This trend continues until around 8pm when the heating effects of the water wall take over. However, with continuous release of the stored heat, the ability of the water wall to maintain the ventilation of the solar chimney and to heat the room keeps declining. Consequently, as can be observed in Figure 3 (d) and Figure 4 (d), at around midnight, reverse flow offsets the ventilation effects and at the same time room temperature starts to decrease.

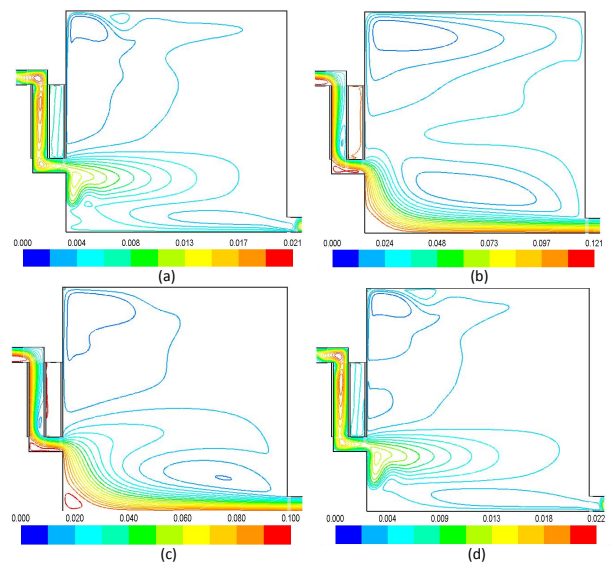


Figure 4. Streamline plots at (a) sunrise, (b) midday, (c) sunset and (d) midnight

Effect of Air Gap Width

Considering that air flows in the chimney channel are essentially boundary layer flows, the relationship between the air gap width and boundary layer thicknesses has a significant impact on the ventilation rate. In order to account for the effects of the air gap width, CFD calculations are performed on combined systems with different air gap widths and the results are compared with those obtained in the reference case (i.e. with an air gap width=0.2m), as are plotted in Figure 5. It can be seen that, as the air gap width increases from 0.1m to 0.2m, the ventilation rate increases and the room temperature decreases due to the increase of cooling effects. The calculation results show that the daily average ventilation rate and room temperature obtained with an air gap width of 0.1m is 0.9ACH less and 0.36°C higher than the reference case. However, it is interesting to note that, when the air gap width is increased to 0.3m, there exists a time delay for the ventilation rate when compared with that obtained with smaller air gap widths. The phenomenon is related to the development of thermal boundary layers. Similar to what can be observed in the reference case, reverse flow develops near the glazing during the night due to the heat loss to the ambient. As solar radiation increases after sunrise, the reverse flow is gradually suppressed by both the temperature rise of the glazing and the expansion of the thermal boundary layer near the water wall. With the largest air gap width, the glazing and the front wall of the water wall are far apart, leaving the thermal boundary

layer near the glazing much less affected by the thermal boundary layer near the water wall. As a result, it takes longer for the reverse flow to be reduced, and only when the overall buoyancy effects become positive does the ventilation rate start to rise. It is found that with an air gap width of 0.3m, a daily average ventilation rate of 5.1ACH is produced, 0.4ACH more than that obtained with the reference case. It is noteworthy that there is also a time delay for the room temperature response when the air gap width is 0.3m. This phenomenon confirms that the ambient air has a strong cooling effect and thus is closely related to the ventilation rate. The time delay for the ventilation rate also allows more time for the residual solar heat to reside and accrue in the room. As a result, compared with the reference case, the daily average room temperature obtained with an air gap width of 0.3m is 0.36°C higher than that obtained with the reference case.

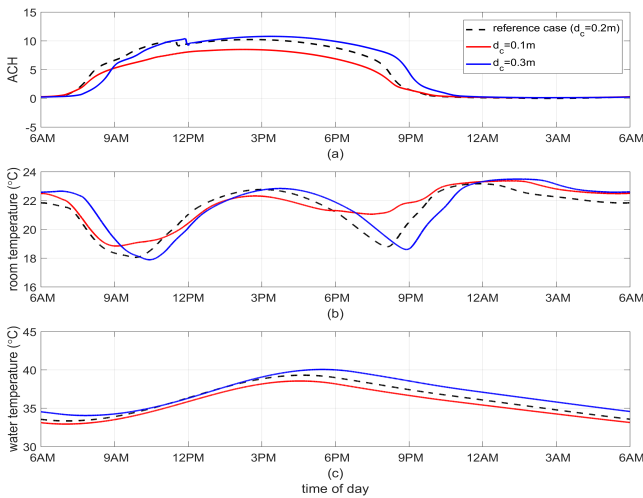


Figure 5. Predicted (a) ventilation rate, (b) room temperature and (c) water temperature for air gap widths ranging between 0.1m and 0.3m

Conclusions

In this paper, a combined solar chimney and water wall is introduced and numerically investigated. The effects of the air gap width on the thermal performance of the combined system are determined through CFD simulations. The daily average results for the ventilation rate (\overline{ACH}), the room temperature (\overline{T}_r) and the water temperature (\overline{T}_w) for each case are summarized in Table 1. Differences between these parameters and those obtained with the reference case ($\Delta\overline{ACH}$, $\Delta\overline{T}_r$, $\Delta\overline{T}_w$) are also listed. Based on the results, the following conclusions can be reached:

- The combined system provides sufficient ventilation for the room and helps to keep the room warm throughout the day and night. Compared with a conventional solar chimney, the combined system sustains the ventilation effects by more than 3 hours after the sunset.
- Increasing the air gap width improves the thermal performance of the system by raising the ventilation rate and increasing the room temperature.
- The air gap width has a significant impact on the ventilation rate, whereas its influence on the room temperature is limited.
- For the winter climate conditions under consideration, it is advisable to adopt relatively small air gap widths to maintain a considerable ventilation rate and a favorable room warmth level.

Air gap width (m)	\overline{ACH} (h ⁻¹)	$\Delta\overline{ACH}$ (h ⁻¹)	\overline{T}_r (°C)	$\Delta\overline{T}_r$ (°C)	\overline{T}_w (°C)	$\Delta\overline{T}_w$ (°C)
0.1	3.8	-0.9 (-19.15%)	21.71	+0.36 (+1.69%)	35.64	-0.59 (-1.63%)
0.2	4.7	-	21.35	-	36.23	-
0.3	5.1	+0.4 (+8.51%)	21.58	+0.23 (+1.08%)	36.94	+0.71 (+1.96%)

Table 1. Summary of CFD results (Results obtained with the reference case are highlighted in bold; percentages in brackets represent the variations relative to the reference case)

References

- [1] H. Wang and C. Lei, Combined Solar Chimney and Water Wall for Ventilation and Thermal Comfort, in *The 4th International Conference On Building Energy & Environment*, Melbourne, Australia, 2018.
- [2] C. Lei, J. Patterson, and M. Lee, Visualisation of natural convection in a reservoir sidearm subject to surface radiation, in *Proc. 7th Australasia Heat and Mass Transfer Conf. Townsville, Australia*, 2000, pp. 201-208.
- [3] M. Rubin, Optical properties of soda lime silica glasses, *Solar energy materials*, vol. 12, pp. 275-288, 1985.
- [4] T. Wu and C. Lei, CFD simulation of the thermal performance of an opaque water wall system for Australian climate, *Solar Energy*, vol. 133, pp. 141-154, 2016.
- [5] W. H. McAdams, *Heat Transmission*, 3rd ed. New York: McGraw-Hill, 1954.
- [6] F. Goia, M. Perino, and M. Haase, A numerical model to evaluate the thermal behaviour of PCM glazing system configurations, *Energy and Buildings*, vol. 54, pp. 141-153, 2012.
- [7] J. P. Abraham and E. M. Sparrow, Three-dimensional laminar and turbulent natural convection in a continuously/discretely wall-heated enclosure containing a thermal load, *Numerical Heat Transfer: Part A: Applications*, vol. 44, pp. 105-125, 2003.
- [8] S. Paitoonsurikarn and K. Lovegrove, Numerical investigation of natural convection loss in cavity-type solar receivers, in *Proceedings of Solar*, 2002, pp. 1-6.
- [9] J. K. Yuan, C. K. Ho, and J. M. Christian, Numerical simulation of natural convection in solar cavity receivers, *Journal of Solar Energy Engineering*, vol. 137, p. 031004, 2015.
- [10] S.-M. Ohk and B.-J. Chung, Natural convection heat transfer inside an open vertical pipe: Influences of length, diameter and Prandtl number, *International Journal of Thermal Sciences*, vol. 115, pp. 54-64, 2017.
- [11] P. Spalart and S. Allmaras, A one-equation turbulence model for aerodynamic flows, AIAA Paper 92-0439, in *30th Aerospace Sciences Meeting and Exhibit*, Reno, NV, U.S.A., 1992, p. 439.
- [12] J. Van Doormaal and G. Raithby, Enhancements of the SIMPLE method for predicting incompressible fluid flows, *Numerical heat transfer*, vol. 7, pp. 147-163, 1984.
- [13] A. Fluent, 12.0 User's guide, *Ansys Inc*, 2009.
- [14] G. A. CIBSE, Environmental design, *The Chartered Institution of Building Services Engineers, London*, 2006.